

REVIEW OF THE COMMON DLR/ONERA PROJECT "ACTIVE TWIST BLADE" (ATB)

Johannes Riemenschneider¹, Stefan Keye¹, Peter Wierach¹, Hugues Mercier des Rochettes²

German Aerospace Center (DLR)

¹ Institute for Structural Mechanics

Braunschweig / Germany

French Aeronautics Center (ONERA)

² DMSE/RCS

Lille / France

Abstract

Individual blade control (IBC) as well as higher harmonic control (HHC) for helicopter rotors promises to be a method to increase flight performance and to reduce vibration and noise. For those controls, an additional twist actuation of the blade is needed. Within the DLR/ONERA partnership, a project called "Active Twist Blade" (ATB) was established on a Joint Team in which two concepts for active twist blades are investigated. This paper presents an overview of the project as well as a description of the two concepts including first demonstrators to prove the feasibility of those activation mechanism.

Introduction and Motivation

The improvement of air traffic around European airports and the circulation of passengers, who reach and leave airports, is a very well known societal need. Helicopters are able to give a positive answer to this need by quickly flying passengers to/from the airport from/to their departure location/final destination in the vicinity of the airport. This requires a new organization of air traffic around airports, minimising interference with large fixed wing aircraft. To maximize airport traffic, the helicopter will require an independent different flight path to the approach and take off of fixed wing flights. At the other end of the helicopter flights are the heliports and vertiports, which are very close to urban areas, where inhabitants require minimum noise. In addition, the helicopter passenger will expect that the comfort level is comparable to that of aeroplanes, which means decrease in helicopter vibrations. Another use of helicopters is Emergency Medical Service (EMS). They require both comfort for passengers and low noise level to be accepted on a long term basis by people living close to hospitals.

The intensive theoretical and experimental work performed both in Europe and the USA shows that BVI (Blade Vortex Interaction) is the most intense noise source and can be dramatically reduced (8 to 10dB) by an appropriate control of the blades at frequencies up to 50Hz (compared to the rotor rotation rate of 4 to 6Hz). The BVI appears during some specific flight phases and especially during approach when the helicopter is close to urban areas.

The benefits of HHC and IBC have been demonstrated both theoretically and practically during flight test. Before this highly desirable technique can be developed at a commercial level, two milestones must be reached:

- Availability of an actuation technology, able to perform in a rotor blade environment

- Development of a demonstration system proving the noise reduction during flight test.

The goal of the Active Twist Blade (ATB) project is to reach the first milestone by developing a piezo actuation technology capable to modify the shape of the blade by twisting. The results will be assessed by means of laboratory results, noise and vibration simulations, and model rotor wind tunnel tests.

Workplan

The project is subdivided into two phases. The first phase starts with the set up of system specification, followed by conception and computation of the rotor blade structure, including selection of materials and geometries, as well as the calculation of the stiffness and strengths. A special focus is laid on the evaluation of suitable active material systems. The whole development is embedded in an iterative process that is followed by an objective assessment. The goal of this assessment is to evaluate the performance of the active twist concepts with respect to rotor dynamics, stability, aerodynamics, acoustics and piloting. In the end of phase one, a demonstrator – based on a BO105 model rotor blade – will be built for each of the two concepts. Both of them will be tested in centrifugal tests and none rotating wind tunnel tests. According to the results of those tests, one concept will be chosen to be investigated in more detail within phase two. Phase two comprises the development and manufacturing of a model scale rotor blade of 4.2 m diameter as well as the testing in the DNW-LLF wind tunnel. Each phase is set out to take 2 years. Phase one is in progress right now. Involved partners are: DLR/FT, DLR/SM, ONERA/DDSS, ONERA/DAAP and ONERA/DSNA.

Details on Concept 1:

Nomenclature

A	Cross sectional area of box beam
a	Thickness of rectangular cross section
b	Width of rectangular cross section
c	Circumference of box beam
d_{ij}	Piezoelectric constants
E	Electric field
F	Force for ATBx experiment
G-I	Torsional rigidity
K_{ij}	Effective laminate stiffness
L	Length of ATBx
M	Moment introduced for twist
s	Deflection
U_{pp}	Voltage; peak-to-peak
α	Twist angle
Θ	Twist angle of Box

The Two Concepts

The concepts under investigation are the Active Twist Blade (ATB) featuring a non-isotropic skin and distributed actuation, and the Twistable Section Closed by Actuation (TWISCA). The paper gives an overview of both concepts and presents the current status of work.

Concept 1 (ATB):

The first concept comprises the implementation of distributed actuation into the blade skin. In order to maximize the resulting twist within given boundary conditions such as torsional rigidity and given actuator design, this concept takes advantage of non-isotropy within the rotor blade skin material. That way, a combination of pure shear and tension-torsion coupling produces more twist than each one of these effects alone (eg. [1]). Previous approaches with distributed actuation only used actuators operating in $\pm 45^\circ$ direction with quasi-isotropic composites ([3]; [4] et al.). Up to now a detailed FE-Model of the blade has been developed and validated using a test structure with simplified geometry. The design of the final demonstrator is completed and the manufacturing of the model blade is in process.

Concept 2 (TWISCA):

This concept features an airfoil with a slotted trailing edge. This slot is closed by a shear actuator, which is able to introduce a parallel movement in span direction between the upper and lower skin. This movement generates a twist on the blade. First investigations of a mini demonstrator made of aluminium with a piezoplate (concentrated actuation and open section) and a rectangular spar show a good correlation between tests and FEM calculation about frequency modes and actuation work. Some tests with a T-spar have shown that it is possible to improve the working behaviour of the proposed concept. The next steps will include the manufacturing and testing of shear actuators and the design of an active blade section with validation by FEM calculation.

Introduction:

The starting point for this concept was a preliminary study on structural properties [2] for the blade skin. Different skin set-ups and materials were compared in a numerical investigation of a thin walled box beam, consisting of either carbon or glass fiber reinforced polymers (CFRP/GFRP) and an active material with directional actuation. Some exemplary results are shown in Figure 1. It was found that for equal torsion stiffness carbon fiber produces higher twist deflections than glass fiber and unidirectional fiber yields higher twist than fabric. Obviously, thinner layer set-ups of the passive material produce lower torsion rigidity but at the same time show a higher active twist.

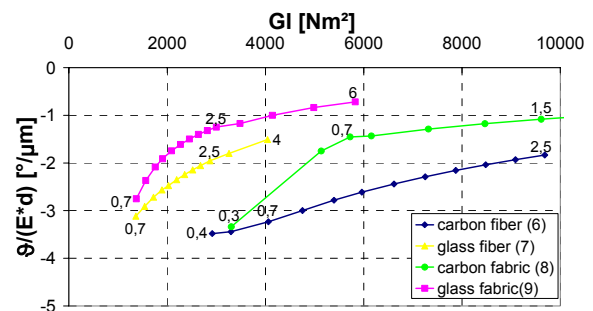


Figure 1: Torsion Stiffness and Twist Angle; Different Materials; Thickness Ratios (of Passive to Active Material) are Plotted at the Data Points

Before the final demonstrator of phase one will be designed and built, basic investigations are performed using a test structure with a simplified cross section. This demonstrator is called “Active Twist Box” (ATBx; Figure 3).

According to the initial investigations described above, a more detailed layout of a thin walled active beam was designed and built in order to validate the finite-element modeling with experimental data and also to gain experience in the manufacturing process of the blade skin. Looking at Figure 1 it appears most effective to use unidirectional CFRP as passive material, since a thin layer thickness would be sufficient to reach the required torsion rigidity. At the same time there is a minimum thickness of available prepreg material with sufficient strength – especially for unidirectional material. This limit is at $\frac{1}{4}$ mm for both CFRP and GFRP.

Active Twist Box:

The purpose of this demonstrator is to validate the finite-element model and to test and develop the manufacturing technology, especially the integration of the actuation system into the composite skin. The simplified shape and design of the demonstrator enables easy, fast and cheap manufacturing and allows to investigate the performance of different configurations. The ATBx demonstrator consists of the skin, the actuation system and a foam core but does not incorporate a spar. The geometry of the test structure was chosen such that the structural properties are similar to the model rotor blade. The main requirement was to

match the torsion stiffness of ATBx to the rotor blade profile. Looking at the basic equation for the effective rigidity (G-I) of a thin walled box beam, we find:

$$GI = \frac{4A^2}{c^2} \oint_c K_{22} ds$$

where A is the surrounded cross-sectional area of the beam, c is the circumference and K_{22} is part of the effective laminate stiffness. K_{22} includes the skin properties, i.e. thickness and material parameters, whereas the factor A^2/c characterizes the cross-section geometry.¹ To obtain equal torsion stiffness for identical skin properties the ATBx cross-section has to be chosen such that the factor A^2/c matches that of the NACA 23012 profile.

Figure 2 is showing the aspect ratio of a rectangular cross section (dimensions a and b), reaching the same factor as the NACA 23012 profile.

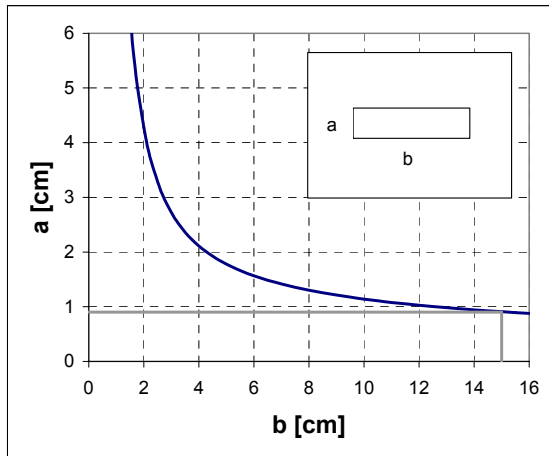


Figure 2: Cross Sectional Dimensions Matching the A^2/c of the NACA 23012 Blade Profile.

Any combinations of a and b given in Figure 2 would yield to appropriate cross-sections. The one that was finally chosen is given in Figure 3, the cross sectional area and circumference are given in Table 1.

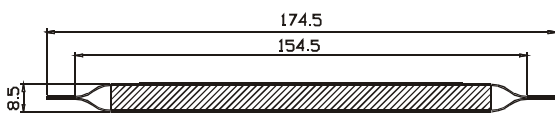


Figure 3: Cross-Section of the ATBx

Cross-Section	$\frac{A}{[m^2]}$	$\frac{c}{[m]}$	$\frac{A^2/c}{[m^3]}$
NACA 0012	1.20×10^{-3}	0.24671	5.83×10^{-6}
NACA 23012	1.20×10^{-3}	0.24697	5.87×10^{-6}
ATBx	1.37×10^{-3}	0.32683	5.74×10^{-6}

Table 1: Geometry data for the ATBx

¹ The second c is reduced with the integral.

According to these geometric requirements a finite-element model was generated and an ATBx was built.

Numerical Simulation:

For modeling the finite-element (FE) code ANSYS was used. In this code the piezoelectric effect is implemented in solid (volume) elements only. Therefore a layered shell element with thermal expansion capability was used: SHELL99. The lengthwise dimension of the box was 1160mm. Three patch type actuators were modeled on the upper and the lower skin of the box at an angle of 30° (see Figure 4). The passive material was modeled as a helical winding with an angle of -40°. The foam in the box was also modeled. Results were obtained for both bending stiffnesses, torsion stiffness, eigenfrequencies and active twist (see Table 3 on page 5). The material data for the CFRP was experimentally derived for the system, which was used for the ATBx, a T300 fiber with Fibredux 913C matrix (fiber volume content of 60%) as a prepreg provided by *HEXCEL composites*.

As boundary conditions all degrees-of-freedom (DoF) were set to zero on one end of the box, and an aluminum plate was modeled at the other side. This plate is needed to introduce forces for the experimental validation.

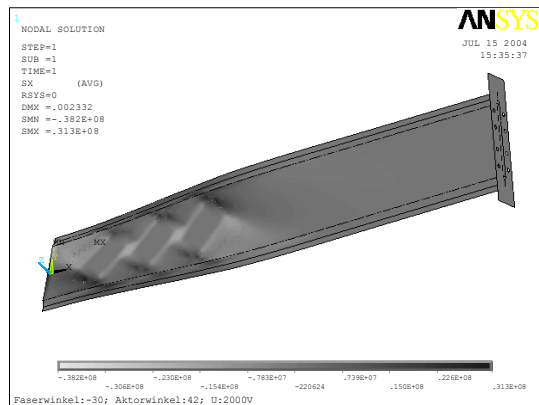


Figure 4: FEM Model of the ATBx; BC: all DoFs are Locked at the Left Edge

Manufacturing of the ATBx:

The ATBx has a length of 1160mm and a width of 174.5mm. Both ends of the demonstrator are equipped with end plates, serving as clamps for lab tests. The location of the MFCs is given in Figure 5.

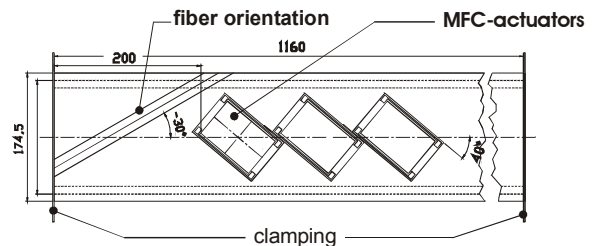


Figure 5: Geometry of the ATBx and Position of the Actuators.

The manufacturing process of the ATBx is conform to the manufacturing process of the final rotor blade

demonstrator and reflects all essential manufacturing steps. This starts with the design of the mold, which is used to manufacture the composite skin. The mold is made of a quasi-isotropic lay up of stitch bonded carbon fiber material from SAERTEX. By using a similar material for the mold and the rotor blade skin, influences of thermal mismatches (differences between the coefficients of thermal expansion) can be reduced. The CFRP mold was built up by a Resin-Transfer-Molding (RTM) process using an aluminum positive core.

The skin itself is made of a carbon fiber prepreg system from HEXCEL composites (Fibredux 913C-T300J(12)-10-35) with an area weight of 409g/m². This results in a thickness of 0,25mm for one cured layer of prepreg, assuming a fiber volume content of 60%. The skin is made of only one layer with a fiber orientation of -30°. Young's Modulus of this material is 142GPa.

Both skins were manufactured separately and bonded together using a cold setting epoxy resin (Araldite 2014). This avoids internal stresses and deformations, which would be caused by a thermosetting resin in combination with the anisotropic skin.

Each side of the ATBx is equipped with three actuators with an orientation of 30°, using standard macro-fiber composite (MFC) actuators from Smart Material Corporation

[5] with an active area of 57x87mm². To improve the adhesion between the composite skin and the actuators, a corona treatment of the actuator surface (polyimid) was applied. Before the actuators were processed, each of them was tested and a strain-voltage curve was recorded to provide reliable performance data.

Overall, five different ATBx configurations were built and tested:

No.	Actuator	Core	Comment
1.1	None	None	diff. geometry an lay up
2.1	None	None	-
2.2	Bonded	None	-
2.3	Bonded	Yes	-
3.1	Embedded	Yes	-

Table 2: ATBx Configurations that were built

In the bonded configuration the actuators were glued to the outer surface using the same cold setting epoxy resin, which has been used for the bonding of the CFRP skins. The thickness of the bonding layer was adjusted to 100µm. In the embedded configuration the actuators were placed on the uncured prepreg before the autoclave process. To protect the actuators and to guarantee a smooth surface, an additional very thin polyester mat with an area weight of 27g/m² was placed on the exterior of the skin.

Experimental Testing:

In order to validate the numerical model, different experimental investigations are carried out and results are compared to the respective analytical data. This allows to assess the suitability and accuracy of the finite-element modeling with respect to stiffness distribution

and the representation of the piezoelectric effect. The comparison will include flap and lag bending stiffness, torsion stiffness and active twist performance.

The flap and lag bending stiffness and torsion stiffness are important design parameters in the development process of a new helicopter blade.² Bending and twisting tests were performed on the Active Twist Box to verify the modeling of the respective analytical stiffness properties. Stiffness was determined by introducing forces to the structure and measuring the resulting deflections.

Bending stiffness was measured using a standard three-point-bending test set-up with the box beam being supported by two steel rails mounted on a seismic foundation. Preliminary investigations indicated marginal visco-elastic material behavior. Therefore, the static bending forces were replaced by quasi-static, homogeneous excitation forces of 1Hz. A LDS V 161 shaker was used and bending forces were controlled using a HBM Q 11 force measurement interface.

Deflections at both the forcing point and support locations were measured with Micro-Epsilon LD 1605-0.5 and LD 1605-4 laser triangulators. The resulting bending deformation was computed from

$$s = s_{FP} - \frac{s_{S1} - s_{S2}}{2}$$

where s_{FP} , s_{S1} , and s_{S2} are the measured deflections at the forcing point and support locations, respectively. Different force levels were used and a good linearity was observed, (see Figure 6 and Figure 7).

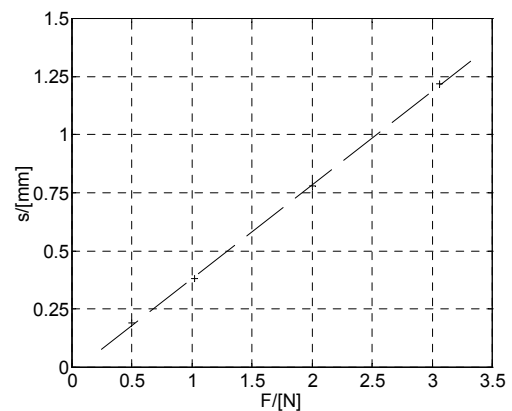


Figure 6: Measured Flap Bending Deflections

² In the ATB research program these parameters have been prescribed to deviate less than ±20% from the existing BO105 rotor blade.

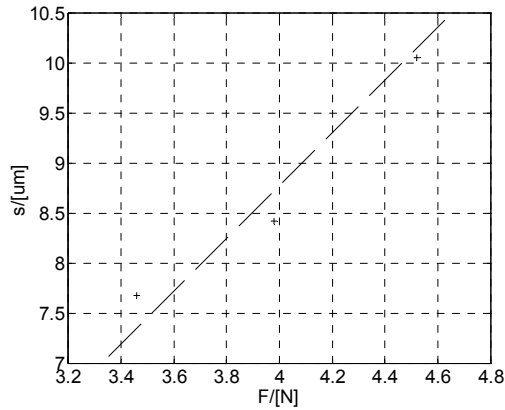


Figure 7: Measured Lag Bending Deflections

Flap and lag bending stiffness was derived from

$$E \cdot I = \frac{F \cdot l^3}{48 \cdot s}$$

and the values listed in Table 3 are based on the mean values of all measurements.

To determine torsion stiffness and to measure the active twist performance the box beams base plate was clamped to a seismic foundation. Torsion moments were introduced into the structure via two nylon strings attached to two bolts in the top plate and a HBM Q 11 force interface was used to measure the string forces.³ The resultant angular deformations were recorded using a laser pointer. Again, linearity was checked by applying different force levels, Figure 8. Torsion stiffness was computed from

$$G \cdot J = 2 \frac{F \cdot l \cdot L}{\alpha}$$

where L is the total length of the active twist box. Results are listed in Table 3.

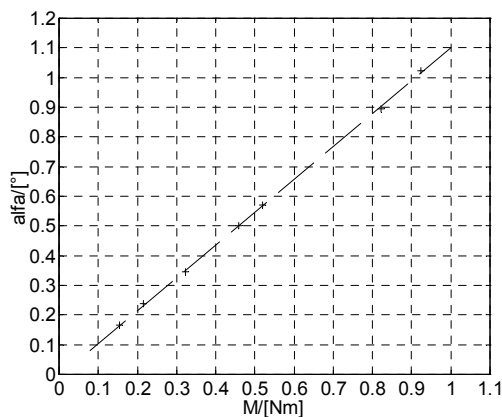


Figure 8: Measured Torsion Deflections

The rotor blades active twisting performance is the leading optimization criterion for both the passive blade structure and the piezoelectric components. To validate the numerical modeling of the piezoelectric effect the

³ With torsion loads the influence of creeping was found to be negligible.

quantitative relation between the voltage applied to the piezoelectric modules and the resulting axial rotation at the free end of the twist box was measured and compared to the finite-element prediction of active twist operation. Again, a quasi-static excitation of 0.1Hz was used to reduce the influence of creeping. The experimental set-up was identical to the one used for the determination of the twist box torsion stiffness. Results are found in Table 3.

Comparison of Analytical and Experimental Data:

Looking at the model there are several possibilities for inaccuracies to enter the model: On one hand there is the passive material: unidirectional CFRP. On the other hand there is the simplification of the piezoelectric effect, which is considered to be linear. Still the model is capable to predict the active twist performance of such a structure, within 10% of the experimental results.

Property	Exp.	Anal.	Deviation
Flap Bending Stiffness	53.65Nm ²	60.90Nm ²	+13%
Lag Bending Stiffness	9445Nm ²	9799Nm ²	+4%
Torsion Stiffness	51.27Nm ²	36.45Nm ²	-29%
1 st Flap Bending Mode	4.14Hz	4.19Hz	+2%
1 st Torsion Mode	50.1Hz	46.26Hz	-6%
Active Twist Deflection	1,3°/2kV	1,2°/2kV	-7%

Table 3: Comparison of Analytical and Experimental Results

Layout of the Model Rotor Blade:

After the validation of the model for the twist box a similar model for a BO105 model rotor blade was lied out (see Figure 9), in order to predict the active twist of a blade, as well as to build up a model for rotor dynamic calculations.

The basic set up of the active skin for this blade is chosen according to the above mentioned analysis as a helical winding of some fiber at an angle of 30° and a layer of actuator patches in an angle of -40°. The spar is supposed to be a C-spar made of GFRP. The stiffness and weight should not go far above that of the passive blade. Strength for this blade has also to be proved for application in a whirl tower (centrifugal loads).

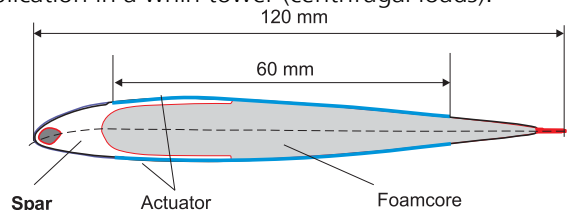


Figure 9: Cross section of the ATB Blade

The highest active twist would be reached using CFRP with a high modulus fiber. Unfortunately the layer thicknesses of the passive material would get very thin

that way. Using a standard T300 carbon fiber for the skin, the target stiffness of the blade (see Table 4) will be overreached by over 85% at a thickness of just 1/8mm. Strength requirements cannot be matched with such a skin either. This might be different for a full scale blade, where the stiffness to be reached is much higher. That is why the model rotor blade has to be designed as a GFRP structure. In those areas, outside the actuator, an additional layer of GFRP is planned to give additional safety against inter fiber cracks. That way, strength requirements will be met. An overview of the properties of that design is given in Table 4.

Property	ATB Blade	BO105
Flap Bending Stiffness	282Nm ²	250Nm ²
Lag Bending Stiffness	6982Nm ²	5200Nm ²
Torsion Stiffness	163Nm ²	160Nm ²
Mass	1,111kg/m	0,95kg/m
EA-to-chord ratio	21,1%	20,5%
CoG-to-chord ratio	24,7%	25%
Active Twist Deflection	+/-1,18°	-
Safety Factor	3,21 (FB)	-
EA: Location of Elastic Achsis		
CoG: Location of Center of Gravity		

Table 4: Properties of ATB Demonstrator (analytical) with Reference Data

Rotor dynamics:

Preliminary rotor dynamic simulations provided an initial overview of the Active Twist Blades performance potential with respect to noise and vibration reduction. Generally, the blade eigenfrequencies are lower than those for the passive BO105 blade which was used as a reference. However, a significant influence only exists for the higher modes, i.e. beyond 9/rev. for $\Omega=1.0$. For noise and vibration simulations a linear twist deformation between 0.0° at the blade root and 0.8° at the tip was chosen for the ATB. The BO105 blade with blade root HHC actuation had a constant angle-of-attack variation of 0.8° over radius. A similar level of both noise (-3dB) and vibration reduction as for the BO105 baseline rotor was predicted for the Active Twist Blade. Additionally, a power reduction of 2.3% at 87m/s ($\mu=0.4$) based on a 2.5to BO105 was computed. As a result the rotor dynamic simulations imply that the performance goals defined in the ATB project will be achieved by the proposed concept.

Details on Concept 2:

The concept principle - acronym TWISCA which means TWIstable Section Closed by Actuation - is based on the principle of a blade opened section with a slot between the upper and lower trailing edge connected to an actuation device which can be of concentrated or distributed type. This actuation produces a parallel movement in span direction between the upper and lower edge; this movement leads to twist the blade as shown on Figure 10.

The type and stiffness of actuation in span direction govern the torsion stiffness level of the blade.

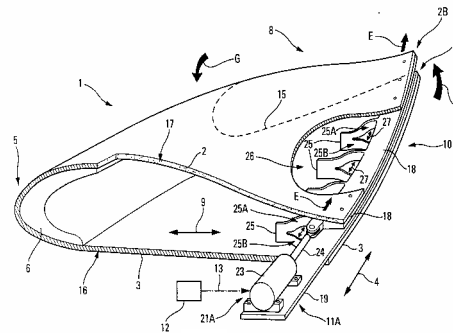


Figure 10: Operational Principle of TWISCA Concept

First investigations have been achieved on a mini demonstrator in order to experimentally check the efficiency of this concept and to rough out the main design parameters ensuring a good working in static and dynamic operation. Finite Elements calculations have been performed in parallel with the tests in order to validate the concept but also the modelling techniques.

First Mini Demonstrator

A first mini demonstrator, presented on Figure 11, was made of aluminium - 130 mm span, 70 mm chord and 2 mm thickness - and included a main spar with a 10*1 mm² rectangular section (R-spar) and two skins of 0.5 mm thickness. A second mini demonstrator was designed with a T-shaped spar in order to test the flap stiffness characteristics.

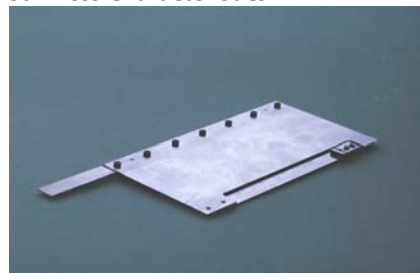


Figure 11: Mini Demonstrator for TWISCA Concept

The actuation, as shown on Figure 12a, is implemented in an open space located on upper trailing edge and is activated by means of a piezoelectric plate working in d13 mode whose dimensions are 80 mm long, 8 mm wid and 1 mm thick (Figure 12b). Each of the plate tips is supported respectively on the upper and lower trailing edge with a light pre-stress. When the piezoelectric plate is supplied, its elongation produces the twist of the sample.

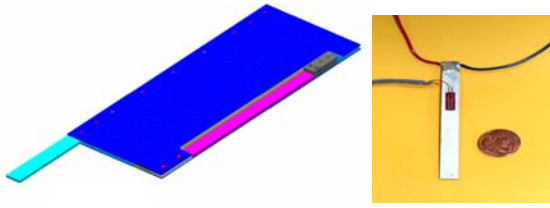


Figure 12: a) Model for Demonstrator and b) Piezoelectric plate

The working characteristic curves of plate are presented on Figure 13 in case of blocking force and on Figure 14 in case of maximum stroke.

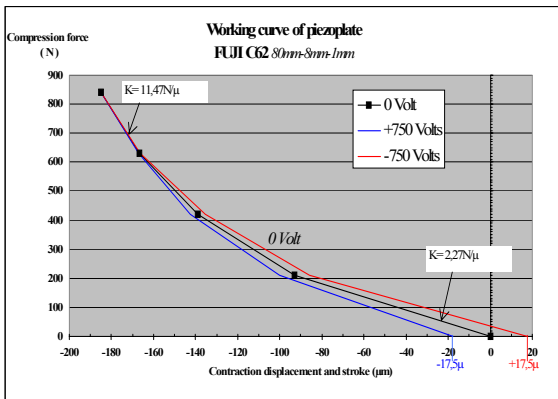


Figure 13: Working Characteristic of Plate in Case of Blocking Force

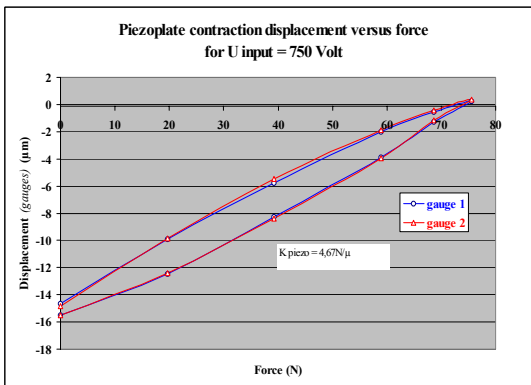


Figure 14: Working Characteristic of Plate in Case of Maximum Stroke

The concept principle consists in letting free the two trailing edges in span direction in order to maximise the tip twist angle. In other way, the blade must be designed with an active outboard part and a passive inboard part, design incompatible with the aforesaid freedom. So in order to seize this problem, first tests have been performed on the two demonstrators with the actuation working in static operation and considering two cases of root clamping: clamping on spar and clamping on root section. Figure 15 (R-spar) and Figure 16 (T-spar) show that the tip twist angle versus the piezoelectric plate supply is not dramatically affected by the clamping conditions. The loss of twist stroke measured for the two tests is between 11% and 22%.

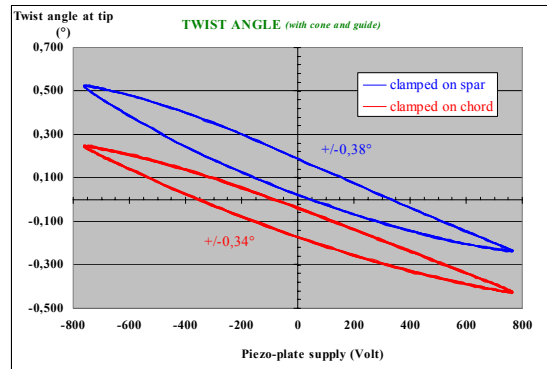


Figure 15: Tip Twist Angle Versus the Piezoelectric plate (R-spar)

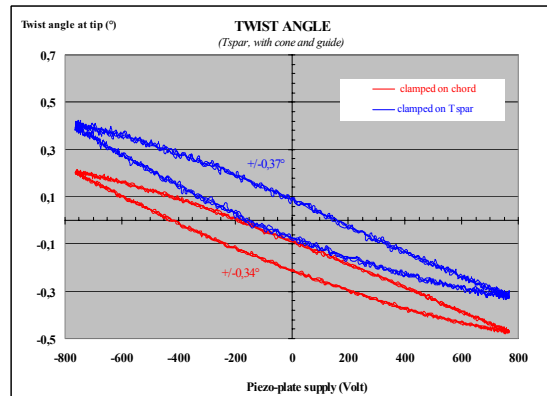


Figure 16: Tip Twist Angle Versus the Piezoelectric Plate (T-spar)

The F.E. calculation performed for the demonstrator with rectangular spar is presented on Figure 17 and Figure 18. Results show 25% more important angle loss with the twist span distribution quasi linear for a spar clamping and parabolic distribution for root clamping. The loss difference between calculation and tests() could be due to the lack of measurement accuracy.

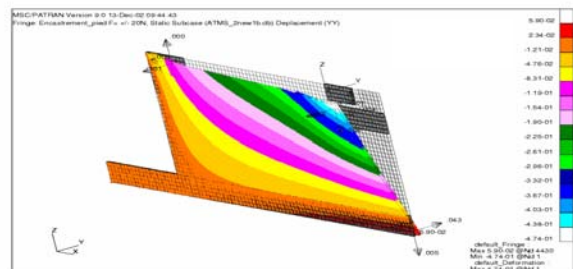


Figure 17: FE Model of Mini Demonstrator Clamped on Spar (1st Eigenfrequency)

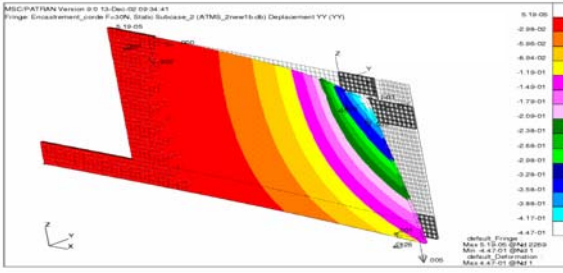


Figure 18: FE model of Mini Demonstrator Clamped on Chord (1st Eigenfrequency)

The natural frequencies and node lines have been measured for the two samples and clamping cases. Frequency results are presented in table below (f= flap and t= torsion). Tests on a reference sample with a closed section and rectangular spar are also mentioned. This table shows the modes coupling between flap and torsion modes connected with the clamping conditions and the inner design.

Natural frequencies in Hertz					
Sample with rectangular spar		Sample with T- spar		reference sample with Closed section rectangular spar	
Clamped on spar	Clamped at root	Clamped on spar	Clamped at root	Clamped on spar	Clamped at root
24.8 f+t	49.9 f+t	51.75 t	71.5 t	28.5 f	80.5 f
62.5 t	148.6 t	116.5 f+t	206.5 t	92 t	274 t
136.5 f+t	286 f		251 f+t		

Table 5: Modes Coupling between Flap and Torsion Modes

For the first mini demonstrator, node lines are plotted on Figure 19 and confirm roughly the FE calculations of natural frequencies presented on Figure 20, according to the clamping cases.

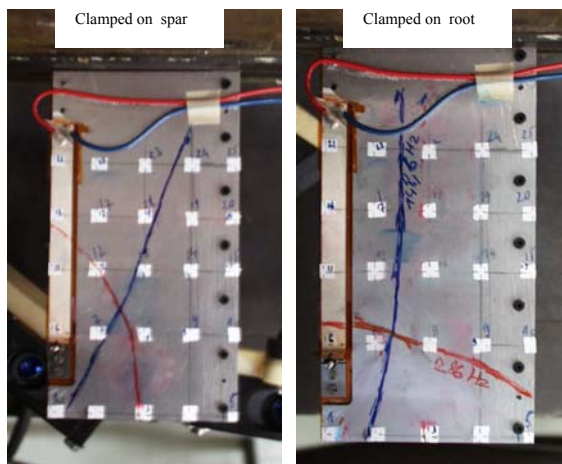


Figure 19: Node Lines for Natural Frequencies for Mini Demonstrator (Clamped on Spar / Clamped on Root)

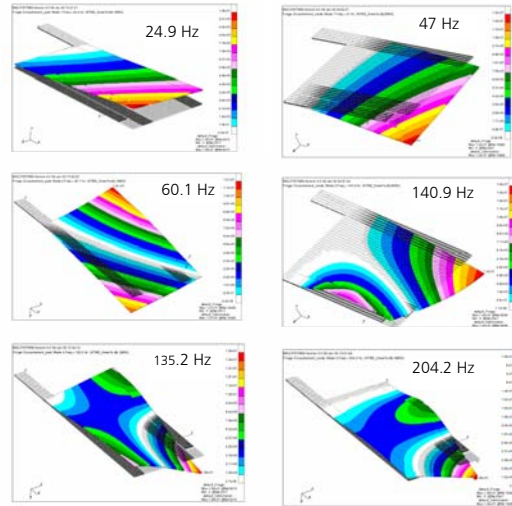


Figure 20: Eigenfrequencies in FE Simulation (Clamped on Spar / Clamped on Root)

Second Mini Demonstrator

For the second mini demonstrator, node lines are plotted on Figure 21 and Figure 22 according to the clamping cases.

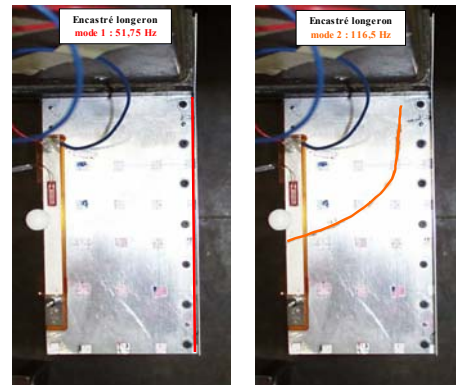


Figure 21: Node Lines for Natural Frequencies for Second Mini Demonstrator (Clamped on Spar)

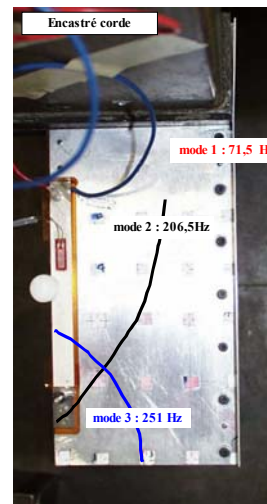


Figure 22: Node Lines for Natural Frequencies for Second Mini Demonstrator (Clamped on Root)

Tests for the actuation working in dynamic operation with a +/-150V supply have been done for the T-spar demonstrator, for the two clamping cases, and show satisfactory results. Amplitudes and phases of tip and root angles are plotted on Figure 23 and Figure 24. The twist angle which is a combination between tip and root rotation amplitudes and phases is more efficient closed to the torsion mode in case of root clamping.

Dynamic tests on the sample with a rectangular spar are in progress and aim at evaluating the effect of the flap mode (located before the torsion mode) on the twist angle efficiency.

For the two samples, the torsion elastic axis is not located on the cg line and some other tests will be done in order to assess this effect on flap torsion coupling.

In conclusion, this study performed on two mini demonstrators shows that the TWISCA concept works correctly and that there is a good agreement between tests and FE calculation.

The next steps will be in one hand to design a shear actuator in order to link continuously the two trailing edges and increase the torsion rigidity of section and in other hand to design a real blade section balanced on cg line and elastic axis.

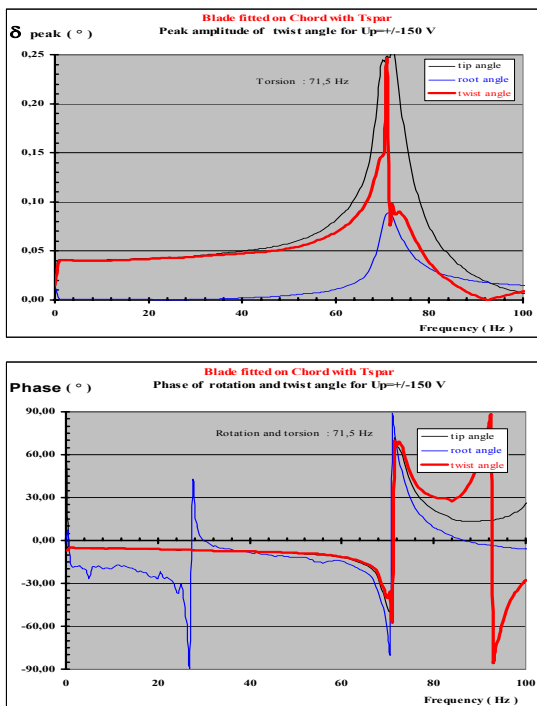


Figure 23: Amplitude and Phase of Twist Angel (blade fitted on Chord with T-spar)

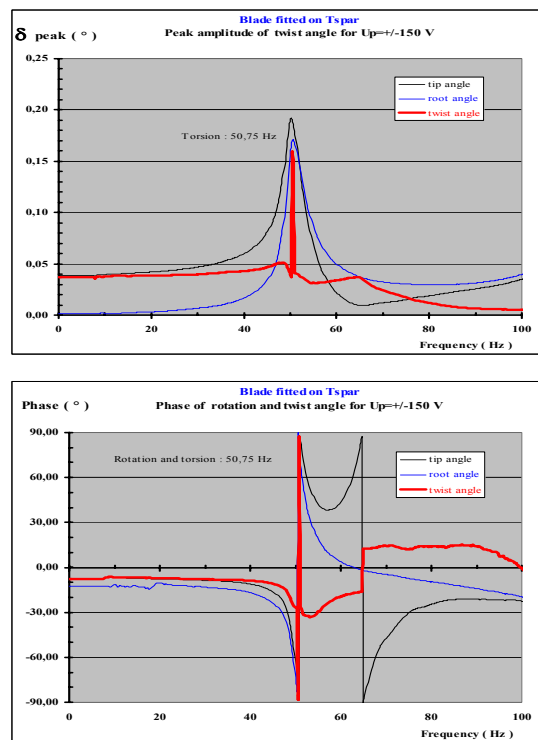


Figure 24: Amplitude and Phase of Twist Angel (blade fitted on T-spar)

References

- [1] Adaptive Blade Twist – calculations and experimental results; Andreas Büter, Elmar Breitbach; *Aerosp. Sci. Technol.* 4 (2000) 309-319
- [2] Preliminary Study on Structural Properties of Active Twist Blades; Johannes Riemenschneider, Peter Wierach, Stefan Keye; 29th European Rotorcraft Forum; Friedrichshafen, Germany; 16.09.2003-18.09.2003
- [3] Derham, Hagood; "Rotor Design Using Smart Materials to Actively Twist Blade"; 52nd Annual Forum of the American Helicopter Society 1996
- [4] Cesnik et al; "Modeling, Desing and Testing of the NASA/ARMY/MIT Active Twist Rotor Prototype Blade"; 55th Annual Forum of American Helicopter Society 1999
- [5] <http://www.smart-material.com>